Hard exclusive pion electroproduction at backward angles with CLAS

K. Park [ai,*], M. Guidal [t], R.W. Gothe [ag], B. Pire [aq], K. Semenov-Tian-Shansky [ar], J.-M. Laget [ai],
K.P. Adhikari [x], S. Adhikari [j], Z. Akbar [k], H. Avakian [ai], J. Ball [e], I. Balossino [o], N.A. Baltzell [ai],
L. Barion [o], M. Battaglieri [q], I. Bedlinskiy [u], A.S. Biselli [h,ac], W.J. Briscoe [m], W.K. Brooks [aj],
V.D. Burkert [ai], F.T. Cao [g], D.S. Carman [ai], A. Celentano [q], G. Charles [ab], T. Chetry [aa],
G. Ciullo [o,i], L. Clark [al], P.L. Cole [n,ai], V. Crede [k], A. D'Angelo [r,ae],
N. Dashyan [ap], R. De Vita [q], E. De Sanctis [p], M. Defurne [e], A. Deur [ai], C. Djalali [ag], R. Dupre [t],
H. Egiyan [ai], A. El Alaoui [aj], L. El Fassi [x], L. Elouadrhiri [ai], P. Eugenio [k], G. Fedotov [aa],
R. Fersch [f], A. Filippi [s], M. Garçon [e], Y. Ghandilyan [ap], G.P. Gilfoyle [ad], F.X. Girod [ai],
E. Golovatch [af], K.A. Griffioen [ao], L. Guo [j,ai], K. Hafidi [a], H. Hakobyan [aj,ap], C. Hanretty [ai],
N. Harrison [ai], M. Hattawy [a], D. Heddle [f,ai], K. Hicks [aa], M. Holtrop [y], C.E. Hyde [ab],
Y. Ilieva [ag,m], D.G. Ireland [al], B.S. Ishkhanov [af], E.L. Isupov [af], D. Jenkins [am], S. Johnston [a],
K. Joo [g,ai], M.L. Kabir [x], D. Keller [an], G. Khachatryan [ap], M. Khachatryan [ab], M. Khandaker [z,1],
W. Kim [w], F.J. Klein [d], V. Kubarovsky [ai], S.E. Kuhn [ab], L. Lanza [r,ae], K. Livingston [al],
I.J.D. MacGregor [al], N. Markov [g], B. McKinnon [al], M. Mirazita [p], V. Mokeev [ai],
R.A. Montgomery [al], C. Munoz Camacho [t], P. Nadel-Turonski [ai], S. Niccolai [t],
G. Niculescu [v,aa], M. Osipenko [q], M. Paolone [ah], R. Paremuzyan [y], E. Pasyuk [ai], W. Phelps [j],
O. Pogorelko [u], J. Poudel [ab], J.W. Price [b], Y. Prok [ab,an], D. Protopopescu [y,2], M. Ripani [q],
A. Rizzo [r,ae], P. Rossi [ai,p], F. Sabatié [e], C. Salgado [z], R.A. Schumacher [c], Y. Sharabian [ai],
Iu. Skorodumina [ag,af], G.D. Smith [ak], D. Sokhan [al], N. Sparveris [ah], S. Stepanyan [ai],
I.I. Strakovsky [m], S. Strauch [ag,m], M. Taiuti [l,3], J.A. Tan [w], M. Ungaro [ai,ac], H. Voskanyan [ap],
E. Voutier [t], X. Wei [ai], N. Zachariou [ak], J. Zhang [an]

[a] *Argonne National Laboratory, Argonne, IL 60439, USA*
[b] *California State University, Dominguez Hills, Carson, CA 90747, USA*
[c] *Carnegie Mellon University, Pittsburgh, PA 15213, USA*
[d] *Catholic University of America, Washington, DC 20064, USA*
[e] *IRFU, CEA, Université Paris-Saclay, F-91191 Gif-sur-Yvette, France*
[f] *Christopher Newport University, Newport News, VA 23606, USA*
[g] *University of Connecticut, Storrs, CT 06269, USA*
[h] *Fairfield University, Fairfield CT 06824, USA*
[i] *Universita' di Ferrara, 44121 Ferrara, Italy*
[j] *Florida International University, Miami, FL 33199, USA*
[k] *Florida State University, Tallahassee, FL 32306, USA*
[l] *Università di Genova, 16146 Genova, Italy*
[m] *The George Washington University, Washington, DC 20052, USA*
[n] *Idaho State University, Pocatello, ID 83209, USA*
[o] *INFN, Sezione di Ferrara, 44100 Ferrara, Italy*
[p] *INFN, Laboratori Nazionali di Frascati, 00044 Frascati, Italy*
[q] *INFN, Sezione di Genova, 16146 Genova, Italy*
[r] *INFN, Sezione di Roma Tor Vergata, 00133 Rome, Italy*
[s] *INFN, Sezione di Torino, 10125 Torino, Italy*

* Corresponding author.
  E-mail address: parkkj@jlab.org (K. Park).
[1] Current address: Pocatello, Idaho 83209, USA.
[2] Current address: Glasgow G12 8QQ, United Kingdom.
[3] Current address: 16146 Genova, Italy.

[t] *Institut de Physique Nucléaire, CNRS/IN2P3 and Université Paris Sud, Orsay, France*
[u] *Institute of Theoretical and Experimental Physics, Moscow, 117259, Russia*
[v] *James Madison University, Harrisonburg, VA 22807, USA*
[w] *Kyungpook National University, Daegu 41566, Republic of Korea*
[x] *Mississippi State University, Mississippi State, MS 39762-5167, USA*
[y] *University of New Hampshire, Durham, NH 03824-3568, USA*
[z] *Norfolk State University, Norfolk, VA 23504, USA*
[aa] *Ohio University, Athens, OH 45701, USA*
[ab] *Old Dominion University, Norfolk, VA 23529, USA*
[ac] *Rensselaer Polytechnic Institute, Troy, NY 12180-3590, USA*
[ad] *University of Richmond, Richmond, VA 23173, USA*
[ae] *Universita' di Roma Tor Vergata, 00133 Rome, Italy*
[af] *Skobeltsyn Institute of Nuclear Physics, Lomonosov Moscow State University, 119234 Moscow, Russia*
[ag] *University of South Carolina, Columbia, SC 29208, USA*
[ah] *Temple University, Philadelphia, PA 19122, USA*
[ai] *Thomas Jefferson National Accelerator Facility, Newport News, VA 23606, USA*
[aj] *Universidad Técnica Federico Santa María, Casilla 110-V Valparaíso, Chile*
[ak] *Edinburgh University, Edinburgh EH9 3JZ, United Kingdom*
[al] *University of Glasgow, Glasgow G12 8QQ, United Kingdom*
[am] *Virginia Tech, Blacksburg, VA 24061-0435, USA*
[an] *University of Virginia, Charlottesville, VA 22901, USA*
[ao] *College of William and Mary, Williamsburg, VA 23187-8795, USA*
[ap] *Yerevan Physics Institute, 375036 Yerevan, Armenia*
[aq] *Centre de physique théorique, École Polytechnique, CNRS, F-91128 Palaiseau, France*
[ar] *National Research Centre Kurchatov Institute, Petersburg Nuclear Physics Institute, RU-188300 Gatchina, Russia*

ARTICLE INFO

ABSTRACT

We report on the first measurement of cross sections for exclusive deeply virtual pion electroproduction off the proton, $ep \to e'n\pi^+$, above the resonance region at backward pion center-of-mass angles. The φ_π^*-dependent cross sections were measured, from which we extracted three combinations of structure functions of the proton. Our results are compatible with calculations based on nucleon-to-pion transition distribution amplitudes (TDAs). These non-perturbative objects are defined as matrix elements of three-quark-light-cone-operators and characterize partonic correlations with a particular emphasis on baryon charge distribution inside a nucleon.

During the past two decades the study of hard exclusive processes has significantly increased the understanding of hadron structure in terms of the fundamental degrees of freedom of Quantum Chromo-Dynamics (QCD), the quarks and gluons. The QCD collinear factorization theorems state that for special kinematic conditions a broad class of hard exclusive reactions can be described in terms of universal nucleon structure functions that depend on variables such as the parton longitudinal momentum fractions and impact parameter, which encode the complex quark and gluon structure of hadrons. Deeply Virtual Compton Scattering (DVCS) off nucleons ($eN \to e'N'\gamma$) and hard exclusive electroproduction of mesons off nucleons ($eN \to e'N'M$) in the generalized Bjorken limit probe the quark and gluon GPDs in the nucleon. The generalized Bjorken limit is defined as sufficiently large lepton momentum transfer squared Q^2 and center-of-mass energy squared $W^2 = m_p^2 + 2m_p\nu - Q^2$ for fixed Bjorken $x_{BJ} = Q^2/(W^2 + Q^2 - m_p^2)$ and small nucleon momentum transfer $|t|$. Here N, N', e and e' denote the initial and final nucleon and the initial and final electron, ν is the electron energy transfer and m_p is the proton mass.

The left panel of Fig. 1 illustrates the reaction mechanism involving GPDs for the $ep \to e'n\pi^+$ process, which provides information on the correlations between the longitudinal momentum and transverse spatial distributions of quarks in the nucleon. GPDs were also found to be a useful probe of parton orbital momentum, which contributes to the nucleon spin. We refer the reader to Refs. [1–4] for the pioneering papers on GPDs and to Refs. [5–10] for reviews of the most important results in the field. Refs. [11–13] made the case that a collinear factorized descrip-

tion may be applied to exclusive hard electroproduction of mesons for the kinematic regime opposite to that of GPDs, i.e. the generalized Bjorken limit in which Mandelstam $|u|$ rather than $|t|$ is small. In the center-of-mass frame, with the positive direction chosen along the incoming virtual photon, the small $|t|$-regime corresponds to mesons produced in the nearly-forward direction, while in the small $|u|$-regime the mesons are produced in the nearly-backward direction. We will refer to these two distinct regimes as "nearly-forward" and "nearly-backward" kinematics. The universal structure functions accessible in "nearly-backward" kinematics are nucleon-to-meson Transition Distribution Amplitudes (TDAs). On the right panel of Fig. 1 we illustrate the corresponding factorization mechanism involving TDAs for $ep \to e'n\pi^+$. In this case, the non-perturbative part describes a nucleon–meson rather than a nucleon–nucleon transition. At a fixed QCD factorization scale, the nucleon-to-meson TDAs are functions of x_1, x_2 and x_3, the three longitudinal momentum fractions of the quarks involved in the process, the skewness variable ξ and u. Since momentum conservation imposes the constraint $\sum_i x_i = 2\xi$, TDAs depend effectively on only 4 variables.

The information encoded in baryon-to-meson TDAs shares common features with the nucleon distribution amplitudes (DAs) and the GPDs. Nucleon-to-meson TDAs characterize partonic correlations inside a nucleon and provide a tool to study the momentum distribution of the nucleon's baryon density. The nucleon-to-meson TDAs involve the same three-quark light-cone operator as the nucleon DA. However, the TDAs are not restricted to the lowest three-quark Fock state of the nucleon, but are sensi-
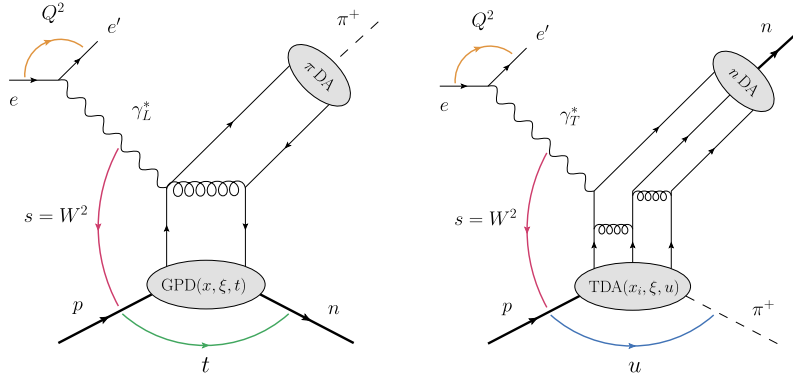
Fig. 1. Left: QCD factorization mechanism for the exclusive electroproduction of a meson (π^+) on the nucleon (proton) in the "nearly-forward" kinematic regime. At large Q^2 and small $|t|$, the amplitude of the process can be presented as a convolution of a hard part calculable in perturbative QCD and two general structure functions parametrizing the complex non-perturbative structure of the nucleon (the GPDs; bottom blob of the diagram) and of the meson (the pion DA upper blob of the diagram). Right: factorization mechanism for the same reaction in the complementary "nearly-backward" kinematic regime, where Q^2 and W^2 are large, x_{BJ} is fixed and $|u|$ is kept small. The amplitude of the process is written as the convolution of the hard interaction amplitude (calculable in perturbative QCD) involving the virtual photon, the three quarks of the out-going nucleon and two gluons, with two structure functions parametrizing the non-perturbative nucleon-to-pion transitions (TDAs) (bottom blob of the diagram) and the nucleon DA (upper blob of the diagram).

tive to $q\bar{q}$-pairs in both the nucleon and meson. Similar to the GPDs (see *e.g.* Ref. [14]), a Fourier transformed TDAs ($\Delta_T \rightarrow \mathbf{b}$) allow an impact-parameter interpretation for TDAs in the transverse plane. Depending on the range of x_i, TDAs either describe the process of kicking out a three-quark cluster from the nucleon at some transverse position **b** or the process of emission of a quark (a pair of quarks) with subsequent re-absorption of a pair of quarks (a quark) by the final-state meson. This yields additional information on nucleon structure in the transverse plane and allows femto-photography of hadrons from a new perspective. We refer the reader to Refs. [15–17].

In this letter, we present the first experimental results that test the nucleon-to-pion TDA formulation. We have analyzed for the first time the $ep \rightarrow e'n\pi^+$ reaction at relatively large Q^2 (> 1.7 GeV^2) and small $\langle |u| \rangle$ ($= 0.5$ GeV^2) above the resonance region ($W^2 > 4$ GeV^2), in nearly backward kinematics where the TDA formalism is potentially applicable. In the one-photon-exchange approximation, the unpolarized exclusive cross section can be factorized as $\sigma(ep \rightarrow e'n\pi^+) = \Gamma_v \times \sigma(\gamma^* p \rightarrow n\pi^+)$.

The virtual photon flux factor Γ_v is given by:

$$\Gamma_v = \frac{\alpha_{em}}{2\pi^2} \frac{e'}{e} \frac{W^2 - m_p^2}{2m_p Q^2} \frac{1}{1 - \epsilon}, \tag{1}$$

where α_{em} is the electromagnetic coupling constant, ϵ is the virtual photon linear polarization parameter $\epsilon = (1 + 2(v^2/Q^2) \times \tan^2(\theta_e/2))^{-1}$ and θ_e is the scattered electron polar angle. The reduced cross section can then be decomposed as

$$\sigma = \sigma_T + \epsilon\sigma_L + \sqrt{2\epsilon(1+\epsilon)}\sigma_{LT}\cos\varphi_\pi^* + \epsilon\sigma_{TT}\cos 2\varphi_\pi^*, \tag{2}$$

where φ_π^* is the azimuthal angle between the electron scattering plane and the hadronic reaction plane (the starred variables are understood to be in the virtual photon–proton center-of-mass frame). The separated cross sections σ_T, σ_L, σ_{LT} and σ_{TT} depend on W, Q^2 and θ_π^*, the polar angle of the π^+. The variable ξ, on which the TDAs depend, can be approximated as $\xi \sim Q^2/(Q^2 + 2(W^2 + \Delta_T^2 - m_p^2))$, where Δ_T is the transverse component of the nucleon-to-pion momentum transfer. The variable Δ_T can be approximated by $|p_\pi^*|\sin\theta_\pi^*$, which is an experimentally equivalent approach, where $|p_\pi^*|$ is the momentum of the π^+. If $Q^2 \gg m_p^2$ and $Q^2 \gg \Delta_T^2$, then $\xi \approx x_{BJ}/(2 - x_{BJ})$, as in DVCS. In the calculation of cross sections via the diagram of Fig. 1-right, the x_i variables on which the TDAs depend are integrated over and are therefore not directly accessible experimentally. This is just as

the calculation of the cross section of the diagram of Fig. 1-left involves an integration over x of the GPDs.

The measurement was carried out with a 5.754 GeV electron beam energy at Jefferson Lab using the CEBAF Large Acceptance Spectrometer (CLAS) [18]. The experimental data were collected with CLAS during the e1-6 run period from October 2001 through January 2002. CLAS was built around six super-conducting coils arranged symmetrically in azimuth, generating a toroidal magnetic field around the beam axis. The six identical sectors of the magnet were independently instrumented with 34 layers of drift chambers (DCs) for charged particle tracking, plastic scintillation counters for time-of-flight (TOF) measurements, gas threshold Cherenkov counters (CCs) for electron and pion separation and triggering purposes, and electromagnetic calorimeters (ECs) for photon and neutron detection and electron triggering. To aid in electron/pion separation, the EC was segmented into an inner part facing the target and an outer part away from the target. CLAS covered nearly the full 4π solid angle for the detection of charged particles. The azimuthal acceptance was maximum at large polar angles and decreased at forward angles. The e1-6 run had the maximal electron beam energy for the JLab accelerator, which allowed us to reach the largest possible Q^2 values and the maximum CLAS torus magnetic field (current $= 3375$ A), which allowed us to achieve the best acceptance and resolution for out-bending charged particles including the backward-angle π^+s. In this analysis, we detected the scattered electron and the final state pion in CLAS. The θ coverage in polar angle ranges from about 8° to 140° for π^+. The exclusivity of the $ep \rightarrow e'n\pi^+$ reaction was established by making a cut around the neutron mass in the missing mass M_X spectrum of the $ep \rightarrow e'\pi^+X$ system. Details of the data analysis are given in Ref. [19] where the same data set and $ep \rightarrow e'n\pi^+$ process was analyzed to extract GPDs, in that case focusing on the forward-angle pions.

Although the kinematics of the particles was a bit different in the present analysis, the general particle identification procedures and the data analysis techniques are the same as in Ref. [19]. Therefore, in the following, we sketch just the main steps of the present data analysis. The CLAS electron trigger required a minimum energy in the EC in coincidence with a CC signal. To improve the electron selection, additional cuts were applied on the EC energy, corresponding to a minimum electron momentum of 0.64 GeV. A z-vertex cut (-80 mm $< z_{vtx} < -8$ mm, target center was at -40 mm) was made around the target location. A cut on the number of photo-electrons in the CC and general geomet-
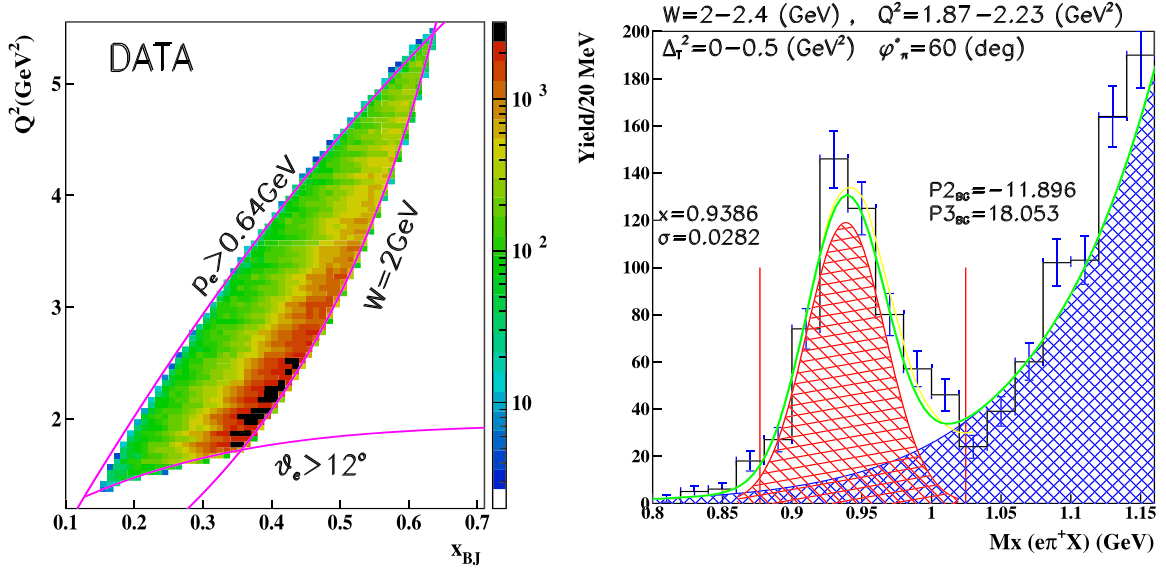
Fig. 2. (Color online.) Left: kinematic coverage in Q^2 versus x_{BJ}. Right: an example of the neutron missing mass peak fit. Here $\langle W \rangle = 2.2$ GeV, $\langle Q^2 \rangle = 2.05$ GeV^2, $\langle \Delta_T^2 \rangle = 0.25$ and $\varphi_\pi^* = 60$ (deg). The red shaded curve (a skewed Gaussian fit) is the signal + radiative tail. The blue shaded curve (exponential + polynomial fit) is the background and the green curve is the sum of both signal and background. Neutrons were selected from the region between the vertical lines.

Table 1
Kinematic bins.

Variable	Number of bins	Range	Bin size
W	1	2.0–2.4 GeV	400 MeV
Q^2	6	1.6–4.5 GeV^2	varying
Δ_T^2	1	0–0.5 GeV^2	0.5 GeV^2
φ_π^*	9	0°–360°	40°

ric fiducial volume cuts were made in order to keep only regions of uniform detector efficiency, which could reliably be reproduced by our Monte-Carlo software/program. Pions were identified by a coincidence of signals in the DC and TOF counters and by the time-of-flight technique within the fiducial cut regions. Missing TOF channels and bad DC regions were excluded from the analysis. All cuts were applied to both experimental and simulated data. Ad-hoc kinematic corrections were used to improve the measured angles and momenta of the particles due to misalignment of CLAS sectors or magnetic field inhomogeneities [20].

The left plot of Fig. 2 shows the kinematic coverage of the data in Q^2 and x_{BJ} after all electron cuts. Two additional cuts, $\Delta_T^2 < 0.5$ GeV^2 and $\cos\theta_\pi^* < 0$, selected backward-angle pions, applicable to the TDA formalism. We binned our phase space trying to keep roughly equal statistics in each bin. Table 1 shows the kinematic bins used in this analysis. The right plot of Fig. 2 shows a typical missing mass M_X spectrum. The background under the neutron missing-mass peak was due to particle misidentification and/or multi-pion channels, smeared by the experimental resolution. This background was estimated by a Gaussian fit to the neutron peak plus an exponential background. Several functions were tested to fit the data. The variation among these fits resulted in a 4% systematic uncertainty. After subtraction, the resulting neutron peak (position and resolution) in the data agreed with the Monte Carlo simulation. The Monte-Carlo software, GSIM, was based on GEANT3 and it is the standard software simulation package for CLAS data analysis. Simulated data go through the same chain of reconstruction codes as real data. Tunable parameters for each detector were adjusted so that the Monte-Carlo distributions matched the experimental data. We used a phase-space-based event generator to simulate $ep \to e'n\pi^+$ [21] with the addition of an exponential e^{Au}-dependence with an ad-hoc param-

eter A to reproduce the pion angular dependence at large angles. The determination of CLAS acceptance and efficiency was done for each four-dimensional bin. The ratio between the number of generated and reconstructed events in a bin, after taking into account all cuts and corrections, was applied as a correction factor. Approximately 300 million $ep \to e'n\pi^+$ events were generated in the kinematic range of Table 1. Radiative corrections were applied using the extended ExcluRad [22] program.

We have extracted the $\sigma_T + \epsilon\sigma_L$ ($= \sigma_U$), σ_{LT} and σ_{TT} cross sections as a function of Q^2 at a given W and $-u$ kinematics. The structure functions σ_U, σ_{LT} and σ_{TT} from the experimental data were fed into the program, and the ratio of the computed cross sections, with radiation on and off, were generated for each bin. The systematic uncertainties associated with this correction were determined using different parameters of the program. This resulted in a 10% systematic uncertainty, which turned out to be the dominant contribution compared to the other systematic uncertainties. The cut values, bin sizes, and fitting functions were varied in order to test the stability of our final cross sections. The systematic uncertainty associated with electron identification was estimated to be less than 2%. For the π^+ identification, the systematic uncertainty is negligible. A one-σ change in the neutron missing mass cut yields an average 3% systematic uncertainty. The Δ_T^2 cut was changed between 0.5 GeV^2 and 1.0 GeV^2, resulting in $< 1\%$ uncertainty. Due to the limited statistics of the experimental data, we used 9 bins in φ_π^*. We tested an analysis with 12 bins in φ_π^*, which resulted in a variation of 4%. The uncertainties associated with the luminosity and the density and length of the target were estimated to be 2% and 1%, respectively. The total systematic uncertainty was estimated to be 12%.

We extracted the φ_π^*-dependent cross sections of the $ep \to e'n\pi^+$ reaction at the average kinematics $\langle W \rangle = 2.2$ GeV and $\langle -u \rangle = 0.5$ GeV^2, for six different Q^2 values: 1.71, 2.05, 2.44, 2.92, 3.48 and 4.16 GeV^2. The data points are included in the CLAS Physics Database [23]. This covers ξ in the range [0.1–0.45]. Fig. 3 shows these results. The differential cross sections are fit to Eq. (2) taking only statistical uncertainties into account. The average χ^2 per degree of freedom of the five lowest-Q^2-bin fits was ~ 2.6 except $Q^2 = 4.16$ GeV^2 due to lack of data. Since the CLAS acceptance showed a complicated φ_π^*-dependence around $\varphi_\pi^* \sim 0$, we
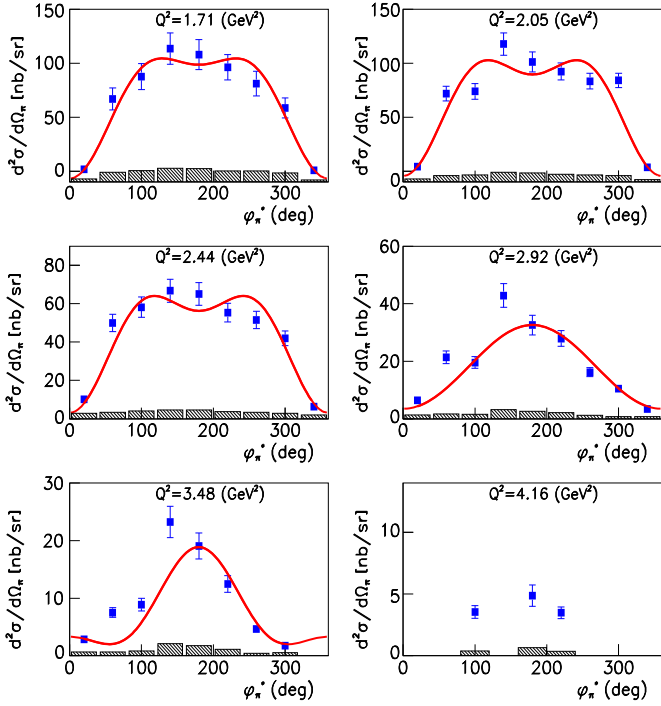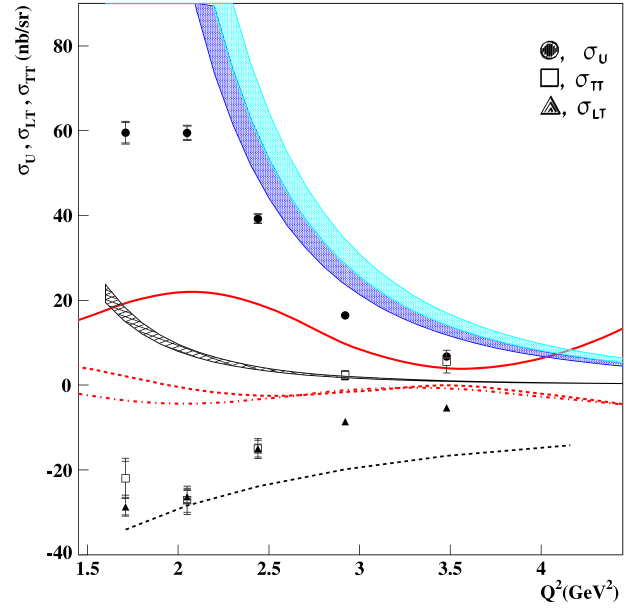
Fig. 3. (Color online.) φ_π^*-dependent differential cross sections ($d\sigma/d\Omega_\pi^*$) for $Q^2 = 1.71$, 2.05, 2.44, 2.92, 3.48, and 4.16 GeV^2 in the backward region. The red solid curves show the full fit results using Eq. (2). The shaded areas show the systematic uncertainty. The Y-axis in the lowest two Q^2 bins has negative offset to show full fit range.

Fig. 4. (Color online.) The structure functions σ_U (•), σ_{TT} (□) and σ_{LT} (▲) as a function of Q^2. The inner error bars are statistical and the outer error bars are total ($= \sqrt{\delta_{stat}^2 + \delta_{sys}^2}$) uncertainties. The bands refer to model calculations of σ_u in the TDA description, black band: BLW NNLO [24], dark blue band: COZ [25], and light blue band: KS [26]. The lower black dashed curve represents an educated guess to a fit of the higher twist cross section σ_{LT} and σ_{TT} in the TDA picture. The red curves are the predictions of [27] for bold solid: σ_U, dashed: σ_{LT}, dot-dashed: σ_{TT}.

took into account an additional systematic uncertainty of φ_π^* binning in the acceptance calculation for extraction of the structure function.

Fig. 4 shows the Q^2-dependence of σ_U, σ_{LT} and σ_{TT}, obtained at the average kinematics $\langle W \rangle = 2.2$ GeV and $\langle -u \rangle = 0.5$ GeV^2. We note that all three cross sections have a strong Q^2-dependence. The TDA formalism predicts the dominance at large Q^2 of the transverse amplitude. Therefore, in order to be able to claim the validity of the TDA approach, it is necessary to separate σ_T from σ_L and check that $\sigma_T \gg \sigma_L$, σ_{TT} and σ_{LT}. With only this set of data at fixed beam energy, we cannot do the experimental separation of σ_T and σ_L. However, we observe that σ_{TT} and σ_{LT} are roughly equal in magnitude and have a similar Q^2-dependence. Their significant size (about 50% of σ_U) implies an important contribution of the transverse amplitude in the cross section. The theoretical TDA description of σ_{TT} and σ_{LT} yields a suppression factor of order Δ_T^2/Q^2 with respect to σ_T. In Fig. 4, we compare our data for σ_U to the theoretical predictions of σ_T from the nucleon pole exchange πN TDA model suggested in Ref. [15]. The curves show the results of three theoretical calculations using different input phenomenological solutions for the nucleon DAs with their uncertainties represented by the bands. Black band: BLW NNLO [24], dark blue band: COZ [25], and light blue band: KS [26]. The black dashed curve, inspired by the higher twist nature of σ_{LT} and σ_{TT} in the TDA picture, shows $(-\Delta_T^2/Q^2)\sigma_U$ parameterized from the experimental data.

The other curves (bold red solid: σ_U, dashed: σ_{LT}, dot-dashed: σ_{TT}) are the predictions of the effective hadronic description of Ref. [27], which is based on the exchange of π- and ρ-Regge trajectories in the t-channel, N- and Δ-Regge trajectories in the u-channel and unitarized π and ρ re-scattering. It reproduces the high energy ($\sqrt{s} = 4$ GeV) SLAC [28] photoproduction data fairly well. When supplemented with t-dependent electromagnetic form factors, according to the prescription of

Ref. [29], it also reproduces the HERMES [30] electroproduction data ($\sqrt{s} = 4$ GeV and $Q^2 = 2.4$ GeV^2). At lower energies ($\sqrt{s} = 2.2$ to 2.5 GeV), this leads to a fair accounting of the published JLab data [19] at low and intermediate t. The model is close to the data at high Q^2 but misses them at lower Q^2.

In summary, we have measured for the first time the cross section of $ep \rightarrow e'n\pi^+$ at large photon virtuality, above the resonance region, for pions at backward angles, using the CLAS detector at Jefferson Lab. The motivation to address such a kinematic regime was provided by the potentially applicable collinear factorized description in terms of nucleon-to-pion TDAs that encode valuable nucleon structural information. The final goal was an experimental validation of the factorized description and the extraction of nucleon-to-pion TDAs from the observed quantities. Our analysis represents a first encouraging step towards this goal. We see a very reasonable agreement between the TDA model-dependent calculation and our data. However, this is not incontrovertible evidence for the validity of the factorized description, since the Regge-based description yields a similar result for the last Q^2 point but a very different Q^2 dependence. From theory, there exists several signs of the onset of factorization. The most obvious ones are the characteristic scaling behavior of the cross section in $1/Q^8$ and the related twist counting rules that lead to the dominance of the transverse polarization of the virtual photon, which results in $\sigma_T \gg \sigma_L$, σ_{LT} and σ_{TT}. Such experimental tests require both the explicit separation of σ_T and σ_L and the precise cross section measurements over a wide range of Q^2 to provide a large lever arm for the $1/Q$-scaling tests. Let us note at this point that the dominance of the transverse cross section was indeed observed in the reaction $\gamma^* p \rightarrow \omega p$ in similar kinematics from Hall-C at JLab [31]. Although the onset of scaling may differ from one reaction to another, this is very encouraging for the reaction that we study where an explicit separation of σ_T and σ_L is urgently needed. Another way to confirm the validity of the factorized description is to use a polarized target to measure the appropriate spin observable.

For example the transverse single spin asymmetry (TSSA) [32] is sensitive to the imaginary part of the reaction amplitude. The considerable size of the TSSA can be most easily interpreted as a sign of the validity of the TDA-based approach. Additional evidence for the TDA-based description can be provided by observing the universality of the nucleon-to-pion TDA accessed in other reactions, which can be studied at $\bar{P}$ANDA@GSI-FAIR [33–36] J-PARC [37] as well as a variety of light meson electroproduction reactions (η, η', ρ) at JLab [38].

Acknowledgements

References

[1] D. Mueller, D. Robaschik, B. Geyer, F.M. Dittes, J. Horejsi, Fortschr. Phys. 42 (1994) 101.
[2] A.V. Radyushkin, Phys. Lett. B 380 (1996) 417.
[3] X. Ji, Phys. Rev. Lett. 78 (1997) 610.
[4] X. Ji, Phys. Rev. D 55 (1997) 7114.
[5] K. Goeke, M.V. Polyakov, M. Vanderhaeghen, Prog. Part. Nucl. Phys. 47 (2001) 401.
[6] M. Diehl, Phys. Rep. 388 (2003) 41.
[7] A. Belitsky, A. Radyushkin, Phys. Rep. 418 (2005) 1.
[8] S. Boffi, B. Pasquini, Riv. Nuovo Cimento 30 (2007) 387.
[9] M. Guidal, H. Moutarde, M. Vanderhaeghen, Rep. Prog. Phys. 76 (2013) 066202.
[10] K. Kumericki, S. Liuti, H. Moutarde, Eur. Phys. J. A 52 (6) (2016) 157.
[11] L.L. Frankfurt, P.V. Pobylitsa, M.V. Polyakov, M. Strikman, Phys. Rev. D 60 (1999) 014010.
[12] B. Pire, L. Szymanowski, Phys. Lett. B 622 (2005) 83.
[13] J.P. Lansberg, B. Pire, L. Szymanowski, Phys. Rev. D 75 (2007) 074004.
[14] R. Dupre, M. Guidal, M. Vanderhaeghen, Phys. Rev. D 95 (1) (2017) 011501.
[15] B. Pire, K. Semenov-Tian-Shansky, L. Szymanowski, Phys. Rev. D 84 (2011) 074014.
[16] J.P. Lansberg, B. Pire, K. Semenov-Tian-Shansky, L. Szymanowski, Phys. Rev. D 85 (2012) 054021.
[17] B. Pire, K. Semenov-Tian-Shansky, L. Szymanowski, Few-Body Syst. 58 (2) (2017) 74.
[18] B.A. Mecking, et al., Nucl. Instrum. Methods A 51 (1995) 409.
[19] K. Park, et al., CLAS Collaboration, Eur. Phys. J. A 49 (2013) 16.
[20] K. Park, et al., CLAS Collaboration, Phys. Rev. C 77 (2008) 015208.
[21] S. Stepanyan, private communication.
[22] A. Afanasev, et al., Phys. Rev. D 66 (2002) 074004.
[23] CLAS Physics Database, http://clasweb.jlab.org/physicsdb.
[24] A. Lenz, M. Gockeler, T. Kaltenbrunner, N. Warkentin, Phys. Rev. D 79 (2009) 093007.
[25] V.L. Chernyak, A.A. Ogloblin, I.R. Zhitnitsky, Z. Phys. C 42 (1989) 583.
[26] I.D. King, C.T. Sachrajda, Nucl. Phys. B 279 (1987) 785.
[27] J.M. Laget, Phys. Lett. B 685 (2010) 146.
[28] R.L. Anderson, et al., Phys. Rev. D 14 (1978) 679;
C. White, et al., Phys. Rev. D 49 (1974) 58.
[29] J.M. Laget, Phys. Rev. D 70 (2004) 054023.
[30] A. Airapetian, et al., Phys. Lett. B 659 (2008) 486.
[31] W. Li, Ph.D. thesis, arXiv:1712.03214, 2017.
[32] J.P. Lansberg, B. Pire, L. Szymanowski, J. Phys. Conf. Ser. 295 (2011) 012090.
[33] J.P. Lansberg, B. Pire, K. Semenov-Tian-Shansky, L. Szymanowski, Phys. Rev. D 86 (2012) 114033; Erratum: Phys. Rev. D 87 (5) (2013) 059902.
[34] B. Pire, K. Semenov-Tian-Shansky, L. Szymanowski, Phys. Lett. B 724 (2013) 99; Erratum: Phys. Lett. B 764 (2017) 335.
[35] B.P. Singh, et al., PANDA Collaboration, Eur. Phys. J. A 51 (8) (2015) 107.
[36] B. Singh, et al., PANDA Collaboration, Phys. Rev. D 95 (3) (2017) 032003.
[37] B. Pire, K. Semenov-Tian-Shansky, L. Szymanowski, Phys. Rev. D 95 (3) (2017) 034021.
[38] B. Pire, K. Semenov-Tian-Shansky, L. Szymanowski, Phys. Rev. D 91 (9) (2015) 094006.